C. R. Geoscience 351 (2019) 190–196

Contents lists available at ScienceDirect

Comptes Rendus Geoscience

www.sciencedirect.com

Internal Geophysics (Physics of Earth's Interior)

Sound velocity of Fe_3C at high pressure and high temperature determined by inelastic X-ray scattering

Suguru Takahashi [a], Eiji Ohtani [a,*], Tatsuya Sakamaki [a], Seiji Kamada [b], Hiroshi Fukui [c,d], Satoshi Tsutsui [e], Hiroshi Uchiyama [e], Daisuke Ishikawa [d,e], Naohisa Hirao [e], Yasuo Ohishi [e], Alfred Q.R. Baron [d]

[a] Department of Earth and Planetary Materials Science, Graduate School of Science, Tohoku University, Sendai 980-8578, Japan
[b] Frontier Research Institute for Interdisciplinary Sciences, Tohoku University, Sendai 980-8578, Japan
[c] Center for Novel Material Science under Multi-Extreme Conditions, Graduate School of Material Science, University of Hyogo, Kamigori, Hyogo 678-1297, Japan
[d] Materials Dynamics Laboratory, RIKEN SPring-8 Center, Sayo, Hyogo 679-5148, Japan
[e] Japan Synchrotron Radiation Research Institute (JASRI), Hyogo 679-5198, Japan

ARTICLE INFO

Article history:
Received 6 May 2018
Accepted after revision 1st October 2018
Available online 14 January 2019

Handled by Guillaume Fiquet

Keywords:
Sound velocity
Fe_3C
High pressure and high temperature
Inelastic X-ray scattering
Core

ABSTRACT

The sound velocity of Fe_3C was measured at pressures from 33 to 86 GPa and at ambient and high temperatures up to 2300 K using inelastic X-ray scattering (IXS) from laser-heated samples in diamond anvil cells (DACs). The compressional velocity (V_P) and density of Fe_3C at room temperature were observed to follow a linear relationship (Birch's law). The temperature dependency of Birch's law was not clearly observed and can be ignored. Birch's law for Fe_3C is expressed by: $V_P = 1.09(\pm0.14)\times\rho - 1.79(\pm1.26)$. The result indicates that V_P and V_S (shear velocity) of the preliminary reference Earth model (PREM) inner core at the Inner Core Boundary (ICB) were by 12% and 48% smaller than those of Fe_3C, which could be accounted for by the premelting effect by analogy from pure Fe or by partial melting of the Fe–Fe_3C mixture in the inner core.

1. Introduction

Seismic velocities such as the compressional velocity (V_P) and shear velocity (V_S) are the most important physical properties of the Earth's interior. The profile of the density and seismic velocity of the Earth's interior have been modeled by seismological observations such as the preliminary Earth reference model, PREM (Dziewonski and Anderson, 1981). Sound velocity measurements of Fe and Fe–light element alloys have been performed under high pressure conditions using various methods, such as shockwave experiments (e.g., Brown and McQueen, 1986), inelastic X-ray scattering (IXS) (e.g., Antonangeli et al., 2004; Mao et al., 2012; Ohtani et al., 2013; Sakamaki et al., 2016), nuclear resonance inelastic X-ray scattering (NRIXS or NIS) (e.g., Lin et al., 2005), impulsive stimulated light scattering (e.g., Crowhurst et al., 2004), and picosecond acoustics (e.g., Decremps et al., 2014). The Earth's inner core is considered to be mainly composed of an Fe alloy with some amounts of light elements to account for the core density deficit (Birch, 1964).

The previous data by NRIXS (Gao et al., 2011) and IXS (Fiquet et al., 2009) are generally consistent with each other up to 50 GPa. However, the measurements by Fiquet

* Corresponding author.
E-mail address: ohtani@m.tohoku.ac.jp (E. Ohtani).

https://doi.org/10.1016/j.crte.2018.09.005

et al. (2009) indicate that the density–V_P relation has an inflection at pressures above 67.4 GPa and that a softening of the dispersion curve appears at 83 GPa. Fiquet et al. (2009) considered that these features might be caused by the magnetic transition at 60 GPa (Vocadlo et al., 2002). However, this transition was reported by Lin et al. (2004) to occur at 25 GPa, and we may need to find another reason for the inflection in Birch's relation. Therefore, it is essential to perform IXS measurements at pressures above 60 GPa and to confirm whether the inflection in the density–V_P curve and magnetic softening exists at around 60–80 GPa. In this paper, we determined the sound velocity values of Fe_3C based on IXS measurements up to 86 GPa and high temperature, and extrapolated the data to the Earth core conditions.

2. Experimental procedure

2.1. Sample preparation

The starting material, Fe_3C, was synthesized from a mixture of Fe and graphite powders by heating at 3 GPa and 1273 K for 12 h using a Kawai-type multianvil apparatus. The starting material of Fe_3C was confirmed to be a single phase of cementite by X-ray diffraction (XRD) and scanning electron microscope (SEM) observations, i.e. it was a single phase of cementite without chemical zoning and interstitial phases.

High pressure was generated using a symmetric-type DAC. Various culet sizes of the diamond anvils from 200 to 350 μm were used, depending on the required experimental pressure conditions. A tungsten gasket was preindented to a thickness of 50 – 70 μm, and an 80 – 120 μm-diameter hole was drilled into the gasket to form the sample chamber. A thin foil of the starting material was made by compressing the Fe_3C chip at room temperature by using opposite anvils (a cold compression technique) and by polishing it to the desired thickness. The XRD pattern of the sample at high pressure shows a clear ring pattern indicating no significant texture effect in the present measurements. A typical two-dimensional (2D) pattern of the sample at high pressure is shown in Fig. 1.

The Fe_3C foil was sandwiched between NaCl layers and was placed in the sample chamber. The NaCl layers served as a pressure-transmitting medium and as a pressure standard for the experiments.

2.2. IXS at SPring-8

The sound velocity of Fe_3C was measured by the IXS method at SPring-8 (Baron, 2010; Baron, 2016; Baron et al., 2000) using a Si (11 11 11) and Si (9 9 9) configuration. The Si (11 11 11) reflection at 21.747 keV provided a resolution of 1.4 meV in a 40 μm × 55 μm beam size. The momentum transfer, $Q = 2\,k_0 \sin(2\theta/2)$, where k_0 is the wave number of the incident photons and 2θ is the scattering angle, was selected by rotating the spectrometer arm in the horizontal plane. In this setup, IXS spectra were collected in the range of $Q = 4.04$–$11.50\ \mathrm{nm}^{-1}$ at each experimental pressure.

The Si (9 9 9) configuration provided an incident photon energy of 17.794 keV with an energy resolution of 2.8 meV full width at half-maximum (FWHM). The X-ray beam size was focused to 16 μm × 16 μm by a Kirkpatrick–Baez (KB) mirror pair. In this configuration, the IXS spectra were obtained in the range of $Q = 7.0$–$10.3\ \mathrm{nm}^{-1}$ at each experimental pressure. The momentum resolution was set to about $0.4\ \mathrm{nm}^{-1}$ full width. two room temperature and two high temperature runs made at 1400 K and 2300 K were conducted on this configuration. We used a portable double-sided laser heating and temperature measurement system (Fukui et al., 2013) combined with a symmetrical DAC for the determination of the sound velocity at high pressure and high temperature at BL35XU. The laser beam size was 20–30 μm in diameter, which was larger than the X-ray beam size (16 μm × 16 μm). We applied a flattop laser beam using a beam shaper.

Spectra were measured for about 8–12 h at room temperature and 6–8 h at high temperature. The shorter

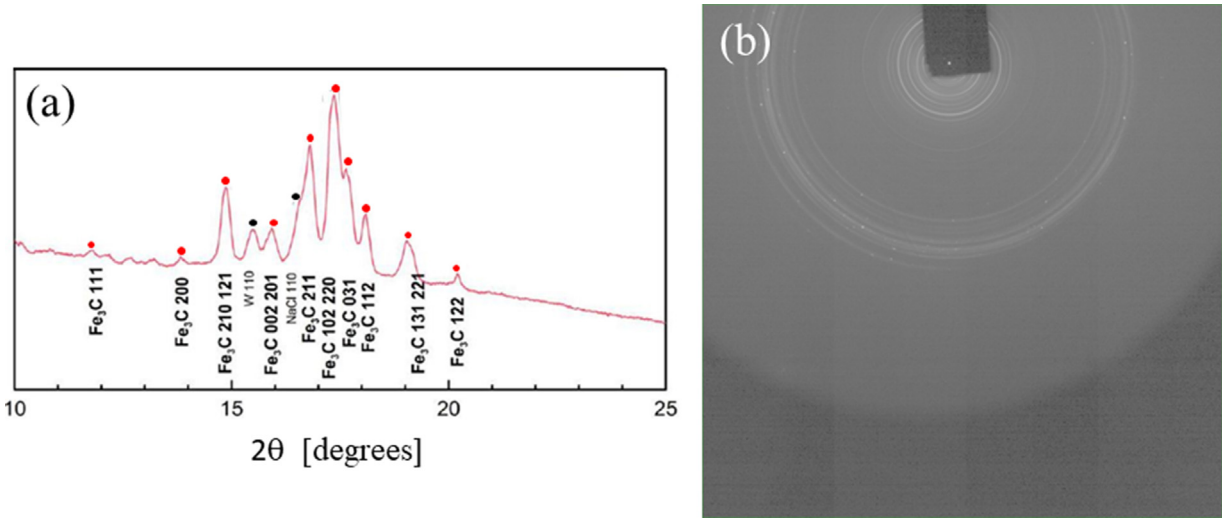

Fig. 1. X-ray diffraction pattern of the sample IXS_Fe_3C_002 (83 GPa and room temperature). (a) One-dimensional and (b) two-dimensional diffraction patterns.

time at high temperature was due to the higher intensity of IXS signals at higher temperature. We monitored the laser heating spot by a charge coupled device (CCD) camera and confirmed that the heating spot was in the correct place of the sample. The position of the laser spot and the heating temperature were controlled during heating and the temperature was recorded every 15 min during the IXS measurements at high temperatures. The fluctuation in temperature was ±200 K during the heating experiments, whereas the temperature gradient at the heating spot was very small by using a flat top beam shaper (Sakamaki et al., 2016). Therefore, the temperature uncertainty was ±200 K at high temperature in the present experiments.

For Fe_3C density determination, XRD patterns of samples were collected using a flat panel (FP; C9732DK, Hamamatsu Photonics K.K.) installed in the IXS optical systems on both setups. The camera length between the sample and the FP was calibrated by a standard crystal of CeO_2.

3. Results

3.1. Measurements of IXS of Fe_3C

IXS measurements were carried out at pressures from 33 to 86 GPa. Typical IXS spectra obtained at 44.4 GPa and 300 K, 40.4 GPa and 1400 K, and 67.4 GPa and 300 K are shown in Fig. 2. The spectrum is characterized by an elastic contribution centered at zero energy and inelastic contributions from Fe_3C and diamond derived from the diamond anvils. The peak of the longitudinal acoustic (LA) phonons of Fe_3C is clearly visible between the peak of the elastic scattering of the sample and the transverse acoustic (TA) phonon of diamond. The LA phonons of diamond would be observed at the higher energy position (e.g., Shibazaki et al., 2012). The energy positions of phonons were extracted by fitting the data with a set of Lorentzian functions. To determine V_P, the obtained phonon dispersion relations of the energy position and momentum transfers were fitted using a sine function as shown below (e.g., Fiquet et al., 2004):

$$E = 4.192\times10^{-4}\times V_P\times Q_{MAX}\times\sin\left(\frac{\pi}{2}\frac{Q}{Q_{MAX}}\right), \quad (1)$$

where E and Q are the energy and the momentum transfer of the phonon obtained by the IXS measurements, respectively. Q_{MAX} corresponds to the first Brillouin zone edge. Typical dispersion curves of Fe_3C for the IXS measurements are shown in Fig. 3. The density of Fe_3C was determined from XRD patterns at each measurement. The values of ρ, V_P, and Q_{MAX} thus determined are summarized in Table 1. The sound velocities in the two set-ups at room temperature were mutually consistent (see Table 1). We also conducted two experiments at high temperatures (1400 and 2300 K). The temperature error of the IXS measurements was typically ±200 K. The Q_{MAX} values might tend to increase with compression. Our data listed in Table 1 generally follow this trend both at room temperature and at high temperature if we consider the errors in Q_{MAX} values determined in this work.

3.2. Birch's law of Fe_3C

The V_P of Fe_3C as a function of the density is shown in Fig. 4. Birch's law of Fe_3C at 300 K was found to be:

$$V_P = 1.16(\pm0.17)\times\rho - 2.51(\pm1.63). \quad (2)$$

We also plotted the sound velocity and density values at high temperatures in Fig. 4. The temperature dependency of Birch's law is not clearly observed and we can ignore it, which is consistent with previous works (e.g., Gao et al., 2011). All data sets of V_P and density relations including 300 K and high temperature were fitted by the following equation:

$$V_P = 1.09(\pm0.14)\times\rho - 1.79(\pm1.26). \quad (3)$$

The V_S of Fe_3C was calculated using the V_P valued determined here. V_S is expressed as follows by using V_P:

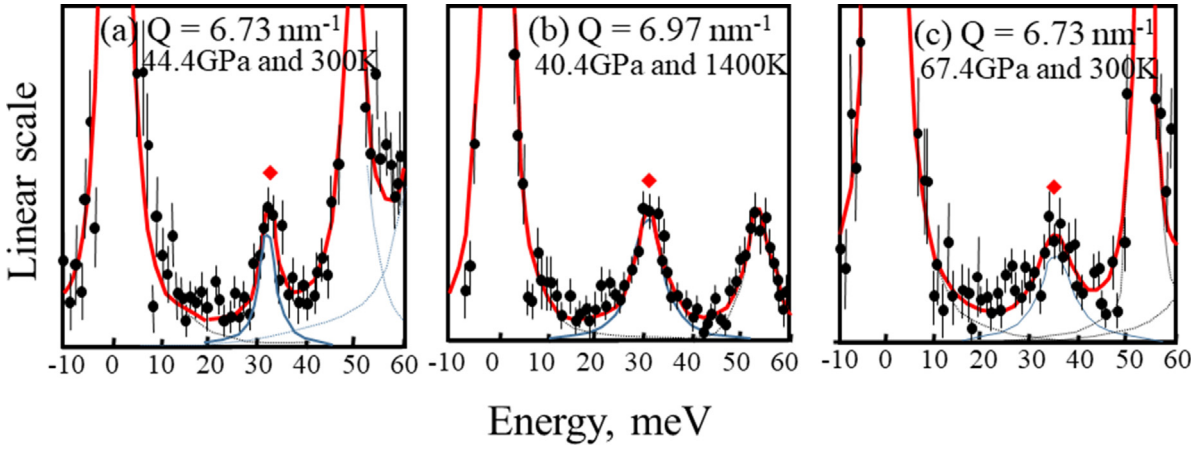

Fig. 2. Examples of the IXS spectra collected at 44.4 GPa and 300 K (a), 40.4 GPa and 1400 K (b), and 67.4 GPa and 300 K (c). LA phonon peaks of Fe_3C (red diamonds), TA phonon peaks of diamond, and elastic peaks are observed. The data are fitted with a set of Lorentzian functions.

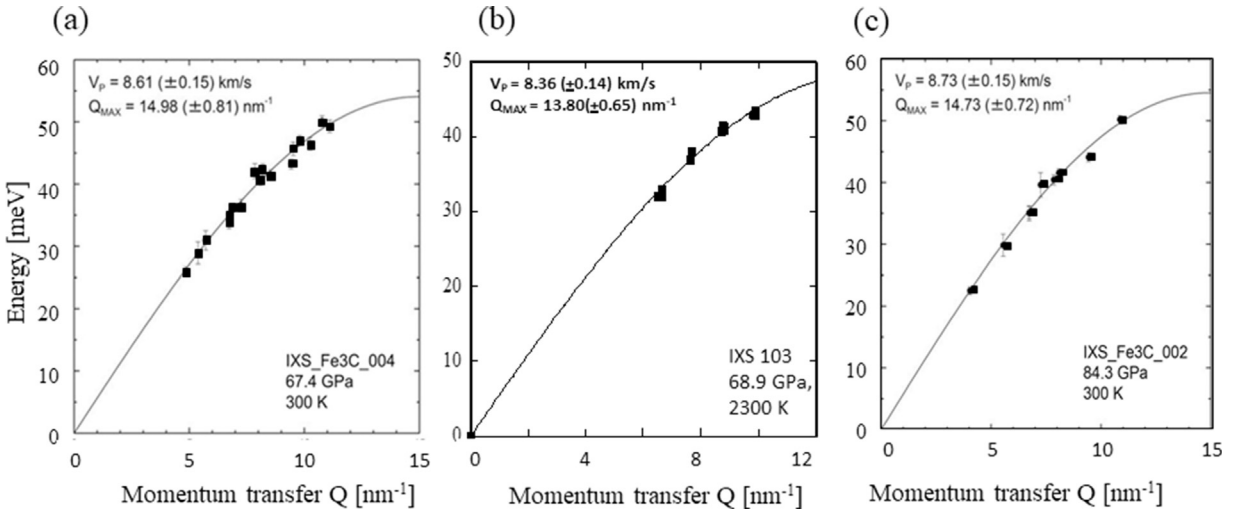

Fig. 3. Dispersion curves obtained at (a) 67.4 GPa, 300 K, (b) 68.9 GPa, 2300 K, and (c) 84.3 GPa, 300 K.

Table 1
Experimental conditions, density, Q_{max}, V_P, and V_S.

Run #	Pressure (GPa)	Error	Temperature (K)	Density (g/cm^3)	Error	Q_{max} (nm^{-1})	Error	V_P (km/s)	Error	V_S (km/s)	Error
(11 11 11)/1.5 meV											
IXS_Fe_3C_002	84.3	1.5	300	9.75	0.02	14.73	0.72	8.73	0.15	3.73	0.27
IXS_Fe_3C_003	44.4	1.2	300	9.02	0.02	13.65	0.61	7.91	0.11	3.30	0.21
IXS_Fe_3C_004	67.4	0.8	300	9.45	0.01	14.98	0.81	8.61	0.15	3.91	0.26
(999)/3meV											
IXS103	68.9	0.7	2300	9.29	0.01	13.80	0.65	8.36	0.14	3.42	0.45
IXS107	32.8	0.9	300	8.78	0.02	13.33	0.4	7.65	0.08	3.20	0.19
IXS108	40.4	1.2	1400	8.77	0.03	12.98	0.36	7.86	0.08	3.42	0.26
IXS115	49.9	1.0	300	9.13	0.02	13.55	0.81	8.25	0.22	3.74	0.37

V_S was calculated using the following parameters: V_0 = 152.13(8) Å^3/unit cell K_0 = 265.1(6) GPa, K' = 3.66(1), $dK/dT = -1.13(5) \times 10^{-2}$, γ_0 = 1.06, q = 1.5 (Takahashi, 2014), V_0 = 149.46A^3, K = 290 GPa, and K' = 3.76 (Sata et al., 2010), $a = (1.8 \sim 4.1) \times 10^{-5}$ K^{-1} (Gao et al., 2011).

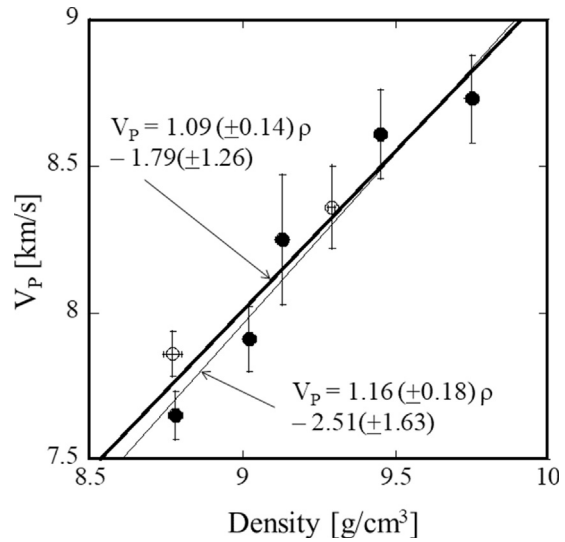

Fig. 4. Density and VP data determined in this work. Solid circles show the data obtained at 300 K at the Si (11 11 11) and Si (9 9 9) configurations. Open circles are the data determined at high temperatures determined at the (9 9 9) configuration. Thick and thin lines show Birch's law for all data and for 300 K only, respectively.

$$V_S = \sqrt{\frac{3}{4}\left(V_P^2 - \frac{K_S}{\rho}\right)}$$

where K_S is the adiabatic bulk modulus and could be approximated by the isothermal bulk modulus K_T based on the following relation, $K_S = K_T(1 + \gamma\alpha T)$. The value of K_T in our experimental conditions was evaluated by the equation of state (EoS) determined in previous works (Sata et al., 2010; Takahashi, 2014) based on the procedure of Anderson (1995); (p. 168, equation 6.30), as it does not increase linearly with pressure. Birch's law for V_S at 300 K was obtained as follows:

$$V_S = 0.63(\pm 0.29) \times \rho - 2.27(\pm 2.71) \quad (4)$$

4. Discussion

4.1. The stability of Fe_3C in the inner core

Nakajima et al. (2009) reported the phase relationships in the Fe–C system up to 30 GPa based on *in situ* XRD experiments using a Kawai-type multianvil apparatus. They found that Fe_3C is stable up to 30 GPa at low temperatures

and that it melts incongruently to form Fe_7C_3 and liquid at higher temperatures. Lord et al. (2009) determined the Fe–Fe_3C eutectic temperature and the melting temperatures of Fe_3C and Fe_7C_3 up to 70 GPa. There were obvious discrepancies with the melting curves of Fe_3C and Fe_7C_3 reported by Nakajima et al. (2009) and Lord et al. (2009). In addition, Lord et al. (2009) predicted that Fe_3C is not stable above about 80 GPa and decomposes into Fe and Fe_7C_3, and suggested that the inner core is composed of Fe + Fe_7C_3. Sata et al. (2010) reported that Fe_3C is stable up to at least 187 GPa at 300 K. Liu et al. (2016) reported that Fe_3C is stable up to about 140 GPa and it decomposes to Fe and Fe_7C_3 at 157 GPa and 2422 K. In contrast, Tateno et al. (2010) and our recent studies (Takahashi, 2014; Takahashi et al., 2013) confirmed the stable existence of Fe_3C at least up to 192 GPa and 4320 K. A recent study on melting experiments in the Fe–Fe_3C system revealed that Fe_3C is present at least up to 150 GPa (Morard et al., 2017). Thus, Fe_3C might exist under the inner core conditions.

4.2. Birch's law of Fe_3C and the sound velocity of Fe_3C under the inner core conditions

Various studies have been conducted on the magnetic transition of Fe_3C. Lin et al. (2004) reported a paramagnetic-to-nonmagnetic transition at around 25 GPa based on X-ray emission spectroscopy (XES). Prescher et al. (2012) reconcile previous investigations and propose that there is a ferromagnetic (fm) to paramagnetic (pm) transition at 10 GPa and a pm to nonmagnetic (nm) transition around 22 GPa. As our IXS measurements cover the pressure range from 32.8 to 84.3 GPa, and Fe_3C is considered to be nm, we can safely extrapolate our results to higher pressures. Based on XES, Chen et al. (2018) claim that the pm–nm transition is completed only at around 50 GPa. Therefore, a low-pressure region in our measurement may contain the effects of pm Fe_3C. Because we assumed the Fe_3C sample is nm in our IXS measurements, our extrapolation to higher pressures could contain an uncertainty.

Fig. 5 shows the comparison of Birch's law of Fe_3C between this and previous studies (Fiquet et al., 2009; Gao et al., 2008; Gao et al., 2011). The slope of our Birch's law is close to that determined by NRIXS (Gao et al., 2011). Although our Birch's law apparently shows a discrepancy from that reported by Fiquet et al. (2009), our data are consistent with theirs, except for the data measured at 68 GPa, which might include an uncertainty. We conducted two measurements of the sample at 67.4 GPa and 68.9 GPa. The dispersion curves are given in Fig. 3a and b. Our sound velocity is smaller than that reported by Fiquet et al. (2009). The X-ray diffraction profile of the sample (Fig. 1) indicates that there is almost no preferred orientation of the Fe_3C sample during compression. Therefore, we cannot specify the cause of difference between our results and those by Fiquet et al. at around 68 GPa. Fig. 3c shows our dispersion curve determined at 84.3 GPa, where Fiquet et al. (2009) reported softening of the dispersion curve. We could not observe such softening of the dispersion curve at this pressure.

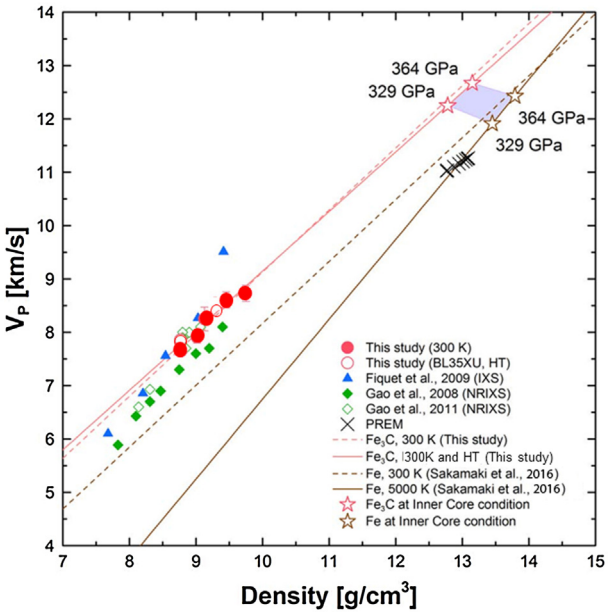

Fig. 5. Comparison of Birch's law of Fe_3C between this study and previous studies (Fiquet et al., 2009; Gao et al., 2008; Gao et al., 2011). Red solid and open circles show the density and V_P profiles by this study at 300 K and high temperatures, respectively. Blue triangles show the results of IXS measurements by Fiquet et al. (2009). Green solid and open diamonds show the results of NRIXS measurements by Gao et al. (2008, 2011). Crosses, × are the plots for the PREM inner core. A red dashed line shows Birch's law of Fe_3C at 300 K, a red line shows Birch's law for the entire data set including those at high temperatures. A brown dashed line is the Birch's law of hcp-Fe at 300 K, a brown line is that extrapolated to 5000 K. Red stars are the values for Fe_3 C at ICB (329 GPa) and at the center of the core (CC, 364 GPa), whereas brown stars are those for hcp-Fe extrapolated to ICB and CC of the Earth. The hatched area represents the data for the V_p and density values for the Fe–Fe_3C mixture.

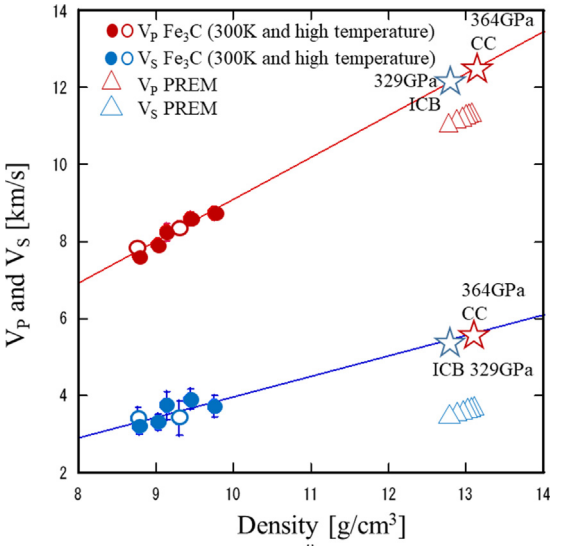

Fig. 6. Birch's law for V_P and V_S of Fe_3C at the ICB and at CC conditions together with those of the PREM inner core at ICB and CC. Present estimations of V_P and V_S of Fe_3C are by 12% and 48% faster than those of the PREM inner core at the ICB, assuming that ICB conditions are 329 GPa and 5000 K (e.g., Terasaki et al., 2011). Red solid circles are the present Birch's law for V_P at room temperature, whereas red open circles are that at high temperature. Blue solid circles are that for the present V_S data at room temperature, whereas blue open circles are that at high temperature. Eqs. (3) and (4) are shown as red and blue lines, respectively. Red triangles are V_P and blue triangles are V_S of the PREM inner core. The blue and red stars are V_P and V_S of Fe_3C at ICB and CC conditions, respectively.

V_P under the ICB condition was determined by Eq. (3). The density of Fe_3C at the inner core condition was calculated by the EoS of Fe_3C (Sata et al., 2010). Here, we ignored the effect of temperature on Birch's law of ρ vs. V_P as our preliminary measurement at high temperature was consistent with that under room temperature conditions. A negligible temperature effect of Fe_3C is consistent with the results by Gao et al. (2011) and Wood et al. (2013), and we used Eqs. (3) and (4) for the ρ–V_P and ρ–V_S relations under the inner core conditions. V_P was plotted as a function of ρ up to the pressure of the center of the Earth's core in Fig. 5. If the inner core is composed of the Fe–Fe_3C system, ρ–V_P should be placed in the shaded area in Fig. 5 assuming that the inner core is the ideal mixture of hcp-Fe and Fe_3C (e.g., Badro et al., 2007). There is no overlap of our extrapolated Birch's law for the V_P data with that of PREM. Thus, it is difficult to explain that the Earth's inner core is composed only of the Fe–Fe_3C mixture.

Fig. 6 shows Birch's law for V_P and V_S of Fe_3C, Eqs. (3) and (4), extrapolated to the inner core boundary (ICB) and to the center of the core (CC), together with those of PREM at ICB and CC. Gao et al. (2011) suggested that the deviation from room temperature Birch's law at high temperature may range from negligible (minimum) to 30%. Our high temperature results shown in Fig. 6 indicate that the deviation at high temperature can be negligible. Present estimations of V_P and V_S of Fe_3C are 12% and 48% faster than those of the PREM inner core at the ICB condition, assuming that ICB is 329 GPa and 5000 K (e.g., Terasaki et al., 2011). The *ab initio* calculations by Martorell et al. (2013) suggested that V_P and V_S of hcp-Fe drop at temperatures close to the melting point, which was called "the premelting effect".

Morard et al. (2017) determined the eutectic temperature of Fe–Fe_3C at the core–mantle boundary (CMB) to be 2950 K, whereas Liu et al. (2016) reported that the solidus temperature at CMB is 3200 K. Extrapolation of both results to ICB conditions by Simon's equation indicates that the solidus temperatures are 3700 and 5000 K, respectively. Thus, the temperature of 5000 K at ICB is close to the Fe–Fe_3C eutectic temperature extrapolated to the ICB pressure. The inner core temperature is close to or exceeds the melting temperature of Fe_3C. Thus, the slower V_P and V_S values of the PREM inner core at ICB compared with those for Fe_3C could be attributed to the premelting effect of Fe_3C by analogy to pure Fe (Martorell et al., 2013), or to the effect of partial melting in the Fe–Fe_3C system. The separation of the partial melt might not be so effective because of its Fe-rich nature compared with that of the solid Fe carbides, although we need a quantitative evaluation of the density difference between the solid and the partial melt in the inner core in future.

Acknowledgement

This work was supported by JSPS KAKENHI Grant No. 22000002 and No. 15H05748 to E.O. The synchrotron radiation experiments were performed under contracts of the SPring-8 Proposal Nos. 2014B1269, 2014B1465, 2015A1539, 2015A1627, 2015B1202, 2015B1334, 2016A1171, 2016B1419, 2017B1214, 20160096, and 20170051.

References

Anderson, O.L., 1995. Equations of state of solids for geophysics and ceramic science. Oxford University Press, New York, 405 p.

Antonangeli, D., Occelli, F., Requardt, H., Badro, J., Fiquet, G., Krisch, M., 2004. Elastic anisotropy in textured hcp-iron to 112 GPa from sound wave propagation measurements. Earth Planet. Sci. Lett. 225, 243–251.

Badro, J., Fiquet, G., Guyot, F., Gregoryanz, E., Occelli, F., Antonangeli, D., d'Astuto, M., 2007. Effect of light elements on the sound velocities in solid iron: implications for the composition of Earth's core. Earth Planet. Sci. Lett. 254, 233–238.

Baron, A.Q.R., 2010. RIKEN Quantum NanoDynamics Beamline (BL43LXU): the next generation for inelastic X-Ray Scattering. SPring-8 Information 15, 14–19.

Baron, A.Q.R., 2016. In: Jaeschke, E.J., Khan, S., Schneider, J.R., Hastings, J.B. (Eds.), High-Resolution Inelastic X-Ray Scattering I&II, in Synchrotron Light Sources and Free-Electron Lasers: accelerator physics, instrumentation and science applications. Springer International Publishing, pp. 1643–1757.

Baron, A.Q.R., Tanaka, Y., Goto, S., Takeshita, K., Matsushita, T., Ishikawa, T., 2000. An X-ray scattering beamline for studying dynamics. J. Phys. Chem. Solids 61, 461–465.

Birch, F., 1964. Density and composition of mantle and core. J. Geophys. Res. 69, 4377–4388.

Brown, J.M., McQueen, R.G., 1986. Phase transitions, Grüneisen parameter, and elasticity for shocked iron between 77 GPa and 400 GPa. J. Geophys. Res. 91, 7485–7494.

Chen, B., Lai, X., li, J., Liu, J., Zhao, J., Bi, W., Ecran Alp, E., Hu, M.Y., Xiao, Y., 2018. Experimental constraints on the sound velocities of cementite Fe_3C to core pressures. Earth Planet. Sci. Lett. 494, 164–171.

Crowhurst, J.C., Goncharov, A.F., Zaug, J.M.J., 2004. Implusive stimulated light scattering from opaque materials at high pressure. J. Phys. Condens. Matter 16, S1137.

Decremps, F., Antonangeli, D., Gauthier, M., Ayrinhac, S., Morand, M., Le Marchand, G., Bergame, F., Philippe, J., 2014. Sound velocity measurements of iron up to 152 GPa by picosecond acoustics in diamond anvil cell. Geophys. Res. Lett. 41, 1459–1464, http://dx.doi.org/10.1002/2013GL058859.

Dziewonski, A.M., Anderson, D.L., 1981. Preliminary reference Earth model. Phys. Earth Planet. Inter. 25, 297–356.

Fiquet, G., Badro, J., Gregoryanz, E., Fei, Y., Occelli, F., 2009. Sound velocity in iron carbide (Fe_3C) at high pressure: implications for the carbon content of the Earth's inner core. Phys. Earth Planet. Inter. 172, 125–129.

Fiquet, G., Badro, J., Guyot, F., Bellin, Ch., Krisch, M., Antonangeli, D., Requardt, H., Mermet, A., Farber, D., Aracne-Ruddle, C., Zhang, J., 2004. Application of inelastic X-ray scattering to the measurements of acoustic wave velocities in geophysical materials at very high pressure. Phys. Earth Planet. Inter. 143–144, 5–18.

Fukui, H., Sakai, T., Sakamaki, T., Kamada, S., Takahashi, S., Ohtani, E., Baron, A.Q.R., 2013. A compact system for generating extreme pressures and temperatures: an application of laser-heated diamond anvil cell to inelastic X-ray scattering. Rev. Sci. Inst. 84, 113902.

Gao, L., Chen, B., Wang, J., Alp, E.E., Zhao, J., Lerche, M., Sturhahn, W., Scott, H.P., Huang, F., Ding, Y., Sinogeikin, S.V., Lundstrom, C.C., Bass, J.D., Lie, J., 2008. Pressure-induced magnetic transition and sound velocities of Fe_3C: implications for carbon in the Earth's inner core. Geophys. Res. Lett. 34, L08303.

Gao, L., Chen, B., Zhao, J., Alp, E.E., Sturhahn, W., Li, J., 2011. Effect of temperature on sound velocities of compressed Fe_3C, a candidate component of the Earth's inner core. Earth Planet. Sci. Lett. 309, 213–220.

Lin, J.F., Struzhkin, V.V., Mao, H.K., Hemley, R.J., Chow, P., Hu, M.Y., Li, J., 2004. Magnetic transition in compressed Fe_3C from X-ray emission spectroscopy. Phys. Rev. B 70 (21), 212405, http://dx.doi.org/10.1103/PhysRevB.70.212405.

Lin, J.F., Sturhahn, W., Zhao, J., Shen, G., Mao, H.K., Hemley, R.J., 2005. Sound velocities of hot dense iron: Birch's law revisited. Science 308, 1892–1894.

Liu, J., Lin, J.-F., Prakapenka, V.B., Prescher, C., Yoshino, T., 2016. Phase relations of Fe_3C and Fe_7C_3 up to 185 GPa and 5200 K: implication for the stability of iron carbide in the Earth's core. Geophys. Res. Lett. 43 , http://dx.doi.org/10.1002/2016GL071353.

Lord, O.T., Walter, M.J., Dasgupta, R., Walker, D., Clark, S.M., 2009. Melting in the Fe–C system to 70 GPa. Earth Planet. Sci. Lett. 284, 157–167.

Ohtani, E., Shibazaki, Y., Sakai, T., Mibe, K., Fukui, H., Kamada, S., Sakamaki, T., Seto, Y., Tsutsui, S., Baron, A.Q.R., 2013. Sound velocity of hexagonal close-packed iron up to core pressures. Geophys. Res. Lett. 40, 5089–5094.

Mao, Z., Lin, J.-F., Liu, J., Alatas, A., Gao, L., Zhao, J., Mao, H.-K., 2012. Sound velocities of Fe and Fe-Si alloy in the Earth's core. Proc. Nat. Acad. Sci. 109, 10239–10244.

Martorell, B., Vočadlo, L., Brodholt, J., Wood, I.G., 2013. Strong premelting effect in the elastic properties of hcp-Fe under inner-core conditions. Science 342, 466–468.

Morard, G., Andrault, D., Antonangeli, D., Nakajima, Y., Auzende, A.L., Boulard, E., Cervera, S., Clark, A., Lord, O.T., Siebert, J., Svitlyk, V., Garbarino, G., Mezouar, M., 2017. Fe–FeO and Fe–Fe_3C melting relations at Earth's core–mantle boundar conditions: implications for a volatile-rich or oxygen-rich core. Earth Planet. Sci. Lett. 473, 94–103.

Nakajima, Y., Takahashi, E., Suzuki, T., Funakoshi, K., 2009. Carbon in the core revisited. Phys. Earth Planet. Inter. 174, 202–211.

Prescher, C., Dubrovinsky, L., McCammon, C., Glazyrin, K., Nakajima, Y., Kantor, A., Merlini, M., Hanfland, M., 2012. Structurally hidden magnetic transitions in Fe_3C at high pressures. Phys. Rev. B 85, 140402(R).

Sakamaki, T., Ohtani, E., Fukui, H., Kamada, S., Takahashi, S., Sakairi, T., Takahata, A., Sakai, T., Tsutsui, S., Ishikawa, D., Shiraishi, R., Seto, Y., Tsuchiya, T., Baron, A.Q.R., 2016. Sound velocity and density of hcp-Fe under Earth's core conditions. Sci. Adv. 2, e1500802.

Sata, N., Hirose, K., Shen, G., Nakajima, Y., Ohishi, Y., Hirao, N., 2010. Compression of FeSi, Fe_3C, $Fe_{0.95}O$, and FeS under the core pressures and implication for light element in the Earth's core. J. Geophys. Res. 115, B09204.

Shibazaki, Y., Ohtani, E., Fukui, H., Sakai, T., Kamada, S., Ishikawa, D., Tsutsui, S., Baron, A.Q.R., Nishitani, N., Hirao, N., Takemura, K., 2012. Sound velocity measurements in dhcp-FeH up to 70 GPa with inelastic X-ray scattering: Implications for the composition of the Earth's core. Earth Planet. Sci. Lett. 313–314, 79–85.

Takahashi, S., 2014. Melting relations of Fe–Fe_3C system and physical properties of Fe3C under high pressure and temperature conditions: Implications for carbon in the Earth's core Dr. Sc. Thesis. Tohoku University http://hdl.handle.net/10097/60452.

Takahashi, S., Ohtani, E., Sakai, T., Mashino, I., Kamada, S., Miyahara, M., Sakamaki, T., Hirao, N., Ohishi, Y., 2013. Stability and melting relations of Fe_3C up to 3 Mbar: implication of the carbon in the Earth's core Abstract of 2013 Fall Meeting. American Geophysical Union, San Francisco, CA, USA, MR11B-05.

Tateno, S., Hirose, K., Ohishi, Y., Tatsumi, Y., 2010. The structure of iron in Earth's inner core. Science 330, 359–361.

Terasaki, H., Kamada, S., Sakai, T., Ohtani, E., Hirao, N., Ohishi, Y., 2011. Liquidus and solidus temperature of a Fe-O-S alloy up to the pressures of the outer core: implication for the thermal structure of the Earth's core. Earth Planet. Sci. Lett. 232, 379–392.

Vocadlo, L., Brodholt, J., Dobson, D.P., Knight, K.S., Marshall, W.G., Price, G.D., Wood, I.G., 2002. The effect of ferromagnetism on the equation of state of Fe_3C studied by first-principles calculations. Earth Planet. Sci. Lett. 203, 567–575.

Wood, B.J., Li, J., Shahar, A., 2013. Carbon in the core: its influence on the properties of core and mantle. Rev. Miner. Geochem. 75, 231–250.